Radboud University Nijmegen

Faculty of Science

Apparent Horizons in Kerr-Vaidya Black Holes

Where to park your rocket next to a rotating, increasingly heavier black hole so you can still return home

Thesis MSc Physics and Astronomy

Supervisor:
dr. Béatrice Bonga

Author:
Anna van Asselt

Second reader:
Prof. Badri Krishnan

Abstract

There are two common ways to define the boundary of a black hole: event and apparent horizons. To track the evolution of a dynamic black hole, the notion of apparent horizons is arguably physically more interesting. However, apparent horizons depend on your choice of time. In earlier work, this was investigated in the spherically symmetric setting[1]. In this thesis, I study this in the more complicated setting of axi-symmetric dynamic black holes. Using both the "normal slicing" of Kerr-Schild coordinates and a "funky slicing": $\tau = t - \alpha z$, I simulated the apparent horizons of Kerr-Vaidya black holes. The simulation was done using the MOTSfinder numerical Python code. The results matched expectations exactly and can be used to learn more about the behaviour of apparent horizons in dynamic black holes.

Abstract in Plain English

In my master's project I calculated the size of rotating black holes as they become heavier. Black holes are objects in space that eat up everything, even light. We use that to determine how big they are: we find the spot where light cannot escape the black hole. The 'normal', more commonly known way to define the size of the black hole is not completely useful in more complicated cases, which is sadly what we find in space. So we use a different way to calculate the size of a black hole, which has its own disadvantages. The calculations were successful, the results behaved exactly like we want them to. This calculation will hopefully help us learn more about these disadvantages and how to work with them, so we can use this method to compute the size of black holes in the future.

August 2026

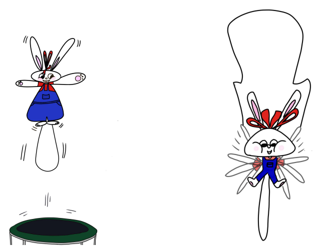

Contents

1 Introduction

Black holes are some of the most mysterious and intriguing objects in the universe. They remain a fascinating research subject, made more difficult by their very essence; how can you research something that literally eats all your data?

One thing you can do is find out how far its "eating-reach" is, that is to say: what is the border at which everything, even light, will be trapped and eventually end up in the black hole? If you happened to pay attention to the news around April 2019 when the first photo of a black hole was released[1], you might have heard this description before and recognize the term: the event horizon[2].

However, the event horizon has a subtle but serious problem for dynamical black holes[3][4]. These are black holes that change through the course of time, for example by accumulating mass. The event horizon is defined as the boundary of the region that can never send a signal out to a point infinitely far away, in both the time and physical sense. Locating it therefore requires knowing the entire evolution of the spacetime: you have to evolve all the way to the end of time to know where it was "today." For numerical simulations, where you build up the spacetime step by step, this makes the event horizon fundamentally impossible to locate in real time. For any observations today, this is of course also completely unrealistic.

The apparent horizon avoids this problem. On any given moment in time, it is defined as the outermost surface on which outgoing light rays are momentarily neither converging nor diverging — a marginally trapped surface[5]. In other words, at a given time, it is the boundary at which all light will be pulled inside the black hole. More on its technical definition will follow in Chapter 2. For now though, the important point is that unlike the event horizon, apparent horizons only require information on one time instant, making it computable as a simulation runs.

The price is that the apparent horizon depends on the coordinates you choose to do the calculation: choose a different way of describing the same spacetime, and the apparent horizon you find can differ, appear, or vanish, even though nothing physical has changed[6]. Only for stationary black holes do the two horizons coincide exactly. Nevertheless, so far, in numerical simulations, apparent horizons appear to be well behaved. The goal of this thesis is to explicitly study the dependence of the apparent horizon on the choice of coordinates and to contrast its behaviour to that of event horizons. In particular, I will look at rotating black holes that increase in weight as time goes on, as these come quite close to the black holes we would observe in the universe.

We would like to know how these apparent horizons behave, so we can use them in our simulations of black holes and gravitational waves. Eventually, these simulations are compared with observations and will hopefully teach us more about the inner workings of the universe. For now though, let's focus on studying the apparent horizons of a rotating increasingly massive black hole[2].

[1] I had been finishing high school at this point, studying for my final exams and preparing to start my bachelor physics and astronomy. So the fact that this is also the subject where I end my current academic chapter is a beautiful full circle for me.

[2] You never know when you'll need to know where you can safely park your rocket next to one.

2 Theory

2.1 General Outline of the problem

In my master's project I've been computing the **apparent horizon** in a Kerr-Vaidya spacetime.

Apparent horizon; why do we want to know?

To do computations with black holes, we need some sense of their size. We even have a definition for that: the event horizon. The horizon around the black hole beyond which even light cannot escape. So anything that passes the event horizon will never be able to get back.

To illustrate that, let's take a look at a Penrose diagram[7] of a simple black hole, as can be seen in figure 1. Penrose diagrams are a way of bringing an infinite spacetime to a finite figure, so the vertical axis shows time from $-\infty$ to ∞ and the horizontal axis shows the radial coordinate from 0 to ∞. The diagonal line running from $t = \infty$ to $r = \infty$ are places in the spacetime infinitely far away, in both the time and physical sense. In Penrose diagrams, light rays always run on a 45° angle, so in the diagram below (Fig 1), the bottom light ray is uninterrupted and goes off on its merry way to infinity. The top light ray is absorbed by the black hole, depicted by the wavy line at the top of the diagram. The event horizon is then defined by the 45° line that separates the light rays that end in the black hole and those that end at infinity.

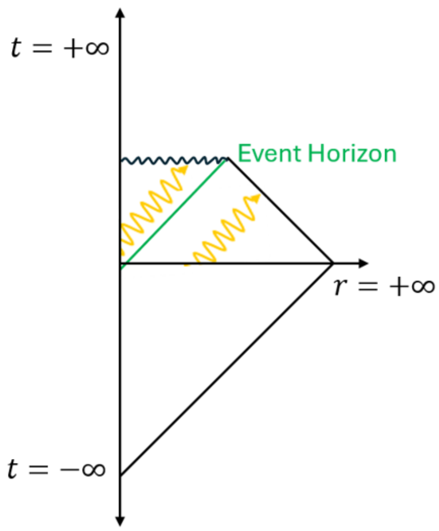

Figure 1: A Penrose diagram of a non-rotating black hole.

This seems like a good enough definition, but it hides a subtlety: the event horizon is defined globally, using the entire future of the spacetime. To see why that's a problem, consider a black hole that forms partway through time — say, from a burst of infalling matter, depicted by the blue line in the diagram below (Fig. 2). Because the event horizon is defined as the boundary of the region that can never send a signal out to infinity, it is a property of the whole spacetime, decided in advance by what will eventually fall in. This means the event horizon at that location already exists before the black hole has actually formed — even in what looks, at that earlier time, like empty flat space. So locating the event horizon "now" requires knowing the full future evolution of the spacetime, all the way to infinity. For dynamical black holes, whose future we don't know in advance (and can't, in a numerical simulation that's still being computed), this makes the event horizon impossible to locate as we go. We need a horizon we can define using only what has already happened — a definition with a shape that reflects the physical situation as it unfolds, like the red line in Fig. 2.

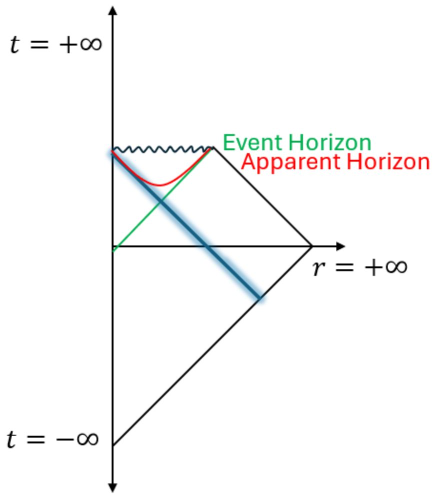

Figure 2: A Penrose diagram of a black hole that is created due to a mass influx, depicted by the blue line.

So we need a different definition for our black hole's horizon. We want something that can (1) be computed without needing to know what the black hole will look like in the future and (2) can change throughout time if the black hole changes. We will use the apparent horizon[3] for this, and as you will see later, it fits both of these requirements.

In layman's terms, the apparent horizon seems really similar to the event horizon. It also describes the points outside of a black hole where light is trapped. But because the mathematical definition is different, it is a much more physically relevant tool in dynamic cases. However, since the world isn't perfect, the apparent horizon also has some downsides. One downside is that the apparent horizon is much harder to compute for each individual time instance than the trivial formula for event horizon in the simplest cases.

The other downside is, in fact, a result of one of our requirements. We require that the apparent horizon can change throughout time, but we are working in general relativity, where time is just one dimension out of four. When we do computations in general relativity, we choose a coordinate system and in that choice we determine what time is. However, that choice can just as easily be along another axis. Since we require that the apparent horizon changes through time, that means that the apparent horizon also changes depending on your coordinate system.

Eventually, we would like to know if the outer edge of all the apparent horizons from all the different coordinate systems will coincide with the event horizon. To do so we first need to compute *some* apparent horizons on *some* different coordinate systems, which is what I have done in this master's project.

2.2 The metric

The metric of choice for this project is the Kerr-Vaidya spacetime, which describes a rotating (Kerr) black hole that absorbs (or, less relevant for physical applications, repels[3]) null dust (Vaidya)[8]. In practice, this means taking the Kerr metric

$$\begin{aligned} ds^2 = &-(1-\frac{2Mr}{\rho^2})dv^2 + 2dvdr - \frac{4aMr\sin^2\theta}{\rho^2}dvd\psi - 2a\sin^2\theta drd\psi + \rho^2 d\theta^2 \\ &+ \frac{(r^2+a^2)^2 - a^2\Delta\sin^2\theta}{\rho^2}\sin^2\theta d\psi^2, \end{aligned} \tag{1}$$

and changing the constant mass to a mass function: $M \rightarrow M(v)$. This gives us the Kerr-Vaidya metric:

$$\begin{aligned} ds^2 = &-(1-\frac{2M(v)r}{\rho^2})dv^2 + 2dvdr - \frac{4aM(v)r\sin^2\theta}{\rho^2}dvd\psi - 2a\sin^2\theta drd\psi + \rho^2 d\theta^2 \\ &+ \frac{(r^2+a^2)^2 - a^2\Delta\sin^2\theta}{\rho^2}\sin^2\theta d\psi^2, \end{aligned} \tag{2}$$

with $\rho^2 = r^2 + a^2\cos^2\theta$, $\Delta = r^2 - 2Mr + a^2$ and $a = J/M$, which describes the angular momentum per unit mass[9].

Unlike Kerr, which is a vacuum solution, the Kerr-Vaidya metric has a non-zero stress-energy tensor corresponding to the incoming null-dust. Some other interesting things to note in this metric are that the rotation occurs around the z-axis with the rotation parameter a. The rotation also causes frame dragging, represented by the $dvd\psi$ term, meaning that the rotation causes a mixing term between the time and azimuthal angle.

2.3 ADM formalism

To calculate the apparent horizon, we need the extrinsic curvature of the metric. This can be calculated using the Arnowitt–Deser–Misner (ADM) formalism, in which a spacetime is divided in a spatial and a time part, also referred to as a (3+1) decomposition. In this section we will dive in the theoretical background of this division and provide some examples. This section is based on [10] and [11].

Before we dive into the math behind the ADM formalism, let's first take a quick look at what it describes. Because decomposing our spacetime into a spatial part and a time part feels a bit antithetical to the spirit of General Relativity.

In the decomposition, we are asking ourselves two questions: (1) if we were able to pause time at a certain point of our choosing, what would our spacetime look like? And (2) after letting time run again for a little while and pausing it again, how has our spacetime changed and what does it look like now? What this essentially creates is a picture book of our spacetime, each page representing a different instant in time, as shown in figure 3.

[3]The repelling case corresponds to a negative mass/energy flux and violates the null energy condition, so it is not physically realizable for a conventional *energy-condition-respecting* source.

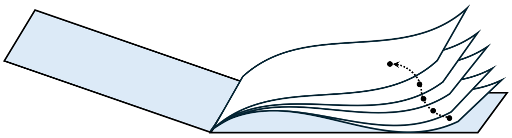

Figure 3: Using ADM formalism, we create a picture book of how space evolves throughout time.

It is important to realise that the pictures in that picture book can be dependent on how we chose to slice our spacetime. Because general relativity unifies space and time into a single four-dimensional spacetime, there's no unique way to split the two apart. Different coordinate systems carve up spacetime into "space" and "time" differently. We use the ADM formalism because it is a calculation tool, but answers arising from its calculations are dependent on the chosen coordinates.

Now, let's take a look at how we mathematically build up our picture book. In the (3+1) decomposition, we take hypersurfaces of constant time, also called timeslices, as depicted in figure 4. Then we use the induced 3-metric γ_{ij} on each of these timeslices as the spatial part of our decomposition. If we now take two hypersurfaces some time dt apart, and define a point on each: p and p', we can introduce two new variables: the lapse, α, and the shift, β_i. The lapse denotes the time difference between the two points. The shift represents how the points are displaced from one hypersurface to another. Both of these variables are freely specifiable gauge choices, not physical fields.

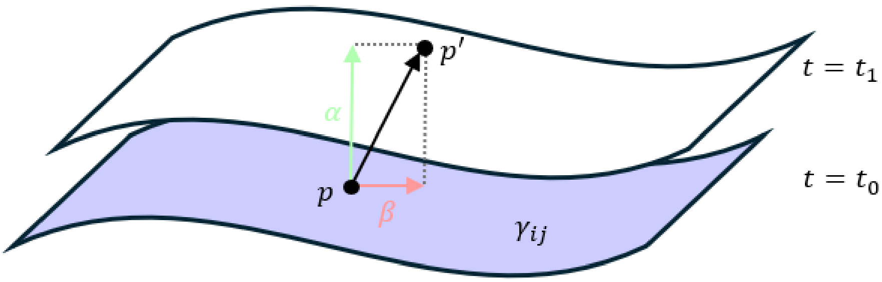

Figure 4: Two hypersurfaces of constant time: t_0 and t_1, with points p and p' respectively. The lapse between them is denoted by α and the shift by β. The induced metric of t_0 is denoted by γ_{ij}.

The original metric can then be written in terms of these ADM-variables as follows:

$$ds^2 = -\alpha^2 dt^2 + \gamma_{ij}(dx^i + \beta^i dt)(dx^j + \beta^j dt). \tag{3}$$

This can be rewritten in a more practical form in the following way. Let's denote the original 4-dimensional metric by $g_{\mu\nu}$ with Greek indices running from 0 to 3. Latin indices only run over the spacial coordinates, going from 1 to 3. Then the induced metric, shift and lapse can be read off from the components of $g_{\mu\nu}$ in the following way:

$$\gamma_{ij} = g_{ij}, \tag{4}$$

$$\beta_i = g_{0i}, \tag{5}$$

$$\alpha^2 = \beta_i \beta^i - g_{00}. \tag{6}$$

Example: Schwarzschild

To bring this into context, we will start by looking at the Schwarzschild spacetime. We start from Schwarzschild in Kerr-Schild coordinates (t, x, y, z), given by:

$$ds^2 = -dt^2 + dx^2 + dy^2 + dz^2 + \frac{2m}{r}(dt + \frac{x}{r}dx + \frac{y}{r}dy + \frac{z}{r}dz)^2. \tag{7}$$

Written in terms of matrix notation, the metric gets the following form:

$$g_{\mu\nu} = \begin{pmatrix} -1 & 0 & 0 & 0 \\ 0 & 1 & 0 & 0 \\ 0 & 0 & 1 & 0 \\ 0 & 0 & 0 & 1 \end{pmatrix} + \frac{2m}{r}\begin{pmatrix} 1 & \frac{x}{r} & \frac{y}{r} & \frac{z}{r} \\ \frac{x}{r} & 0 & 0 & 0 \\ \frac{y}{r} & 0 & 0 & 0 \\ \frac{z}{r} & 0 & 0 & 0 \end{pmatrix} + \frac{2m}{r^3}\begin{pmatrix} 0 & 0 & 0 & 0 \\ 0 & x^2 & xy & xz \\ 0 & xy & y^2 & yx \\ 0 & xz & yz & z^2 \end{pmatrix}. \tag{8}$$

The highlighted parts will determine the ADM-variables. Starting with the induced metric, consisting of all the spatial entries, coloured blue in equation 8. We can write this compactly as:

$$\gamma_{ij} = \delta_{ij} + \frac{2m}{r^3} x_i x_j, \tag{9}$$

where x_i denotes the i-th Cartesian spatial coordinate, e.g. $x_1 = x$ and $x_2 = y$. Its inverse, determined using the Sherman-Morrison formula is:

$$\gamma^{ij} = \delta^{ij} - \frac{2m}{r^3(1 + \frac{2m}{r})} x^i x^j, \tag{10}$$

with the indexes of x^i raised by δ^{ij}. The mixing terms between time and space, coloured red in equation 8, constitute the shift

$$\beta_i = \frac{2m}{r^2} x_i, \tag{11}$$

and its inverse:

$$\beta^i = \frac{\frac{2m}{r^2}}{1 + \frac{2m}{r}} x^i. \tag{12}$$

Using the green matrix elements from equation 8, we can then compute the lapse:

$$\alpha = \frac{1}{\sqrt{1 + \frac{2m}{r}}}. \tag{13}$$

2.4 Funky Slicing

As mentioned before, the (3+1) decomposition of spacetime is dependent on the slicing. Taking a different slicing can give different results, much like calculating the area along a slice of a cube (Fig. 5). In the example above, we used "normal" slicing, taking just the t-coordinate and slicing along that axis. However, we can also slice along different axes, something that in this project I've referred to as "funky" slicing. We do this *because* our calculations are slicing-dependent. By taking different slices over the whole spacetime, we can get a much more complete view of our apparent horizon and eventually also see how close our apparent horizon will reach the event horizon.

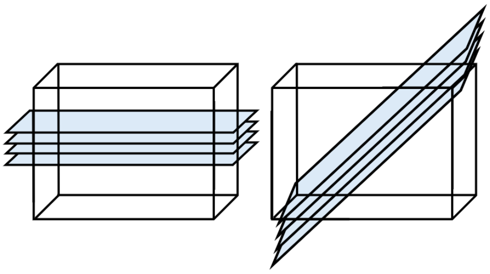

Figure 5: Slicings can be done along any axis, giving a different outcome for each choice of slice.

More specifically, our funky slicing mixes the original t and z-coordinates via $\tau = t - \alpha z$ with a constant parameter α, and takes hypersurfaces of constant τ as our new timeslices. This was chosen because it is simply one of the easiest options to start with, given that the z-axis already a "special axis" because it is also the rotation axis. It would also be interesting to see how $\tau = t - \alpha x$ changes the apparent horizon, since it would be slightly more complicated due to the nature of the Kerr-Vaidya spacetime.

2.5 Extrinsic Curvature

Now let's take a look at how this ADM formalism will help us calculate the apparent horizon. For that, the first step is to take a look at the extrinsic curvature.

So far, we've taken a 4D spacetime and divided it in hypersurfaces, or timeslices. We can now define a future-directed unit normal n^μ on each hypersurface, which will tell us what direction time is running in (Fig. 6). To make it normalized, we define: $n^\mu n_\mu = -1$.

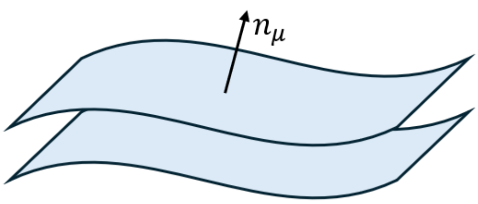

Figure 6: The timelike normal n_μ tells us in which direction time runs

This timelike normal is actually used in the definition of the 3-metric:

$$\gamma_{\mu\nu} = g_{\mu\nu} + n_\mu n_\nu. \tag{14}$$

Now that we have a sense of the direction of time, we can introduce the extrinsic curvature. It will tell us how the 3-metric changes if we move forward in time and how the metric is curved in our 4D spacetime. It is defined as:

$$K_{ij} = -\gamma_i^a \gamma_j^b \nabla_a n_b. \tag{15}$$

The extrinsic curvature in terms of the ADM variables is given by[12]:

$$K_{ij} = \frac{1}{2\alpha}(-\partial_t \gamma_{ij} + D_i\beta_j + D_j\beta_i). \tag{16}$$

Here D_i denotes the covariant derivative with respect to the intrinsic metric γ_{ij}.

Example: Back to Schwarzschild

Since the Schwarzschild spacetime is time-invariant, the extrinsic curvature equation becomes:

$$K_{ij} = \frac{1}{2\alpha}(\partial_i\beta_j + \partial_j\beta_i - 2\Gamma^k_{ij}\beta_k). \tag{17}$$

The resulting extrinsic curvature for the Schwarzschild spacetime with constant t-slices then becomes:

$$K_{ij} = -\frac{2m\sqrt{1+\frac{2m}{r}}}{r^4(r+2m)}((2r+m)x_i x_j - r^3\delta_{ij}). \tag{18}$$

2.6 Expansion

To calculate the apparent horizon, we need to know how light behaves within the spacetime. For that, we need a lightcone. That means we need a second normal vector besides our timelike one: a spacelike normal, s^i (Fig. 7). We can define it like such: $s^i s_i = 1$ and $s^i n_i = 0$, to ensure its orthonormality. This way n^μ and s^i form a 2D surface with null-normals $l^\mu_\pm = n^\mu \pm s^\mu$ so $l^\mu l_\mu = 0$. l_- and l_+ form our light beams, or the edges of a light cone. Later, they will represent the ingoing and outgoing null rays of our black hole.

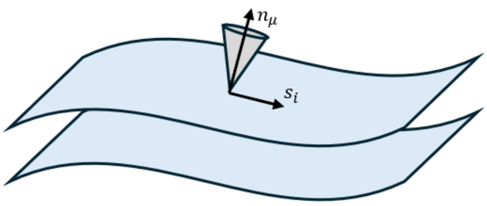

Figure 7: The spacelike normal s_i forms a 2D surface with the timelike normal n_μ.

We can now define expansion: Θ[3][8]. It tells us how much the light rays within our 2D-surface diverge:

$$\Theta_\pm = q^{\mu\nu}\nabla_\mu l_{\pm\nu}. \tag{19}$$

In this equation, $q_{\mu\nu}$ is the induced metric on the 2D-surface between l^μ and n^μ:

$$q_{\mu\nu} = g_{\mu\nu} + n_\mu n_\nu - s_\mu s_\nu. \tag{20}$$

If we now expand equation 19 we get

$$\Theta_\pm = q^{\mu\nu}\nabla_\mu(n_\nu \pm s_\nu) = q^{\mu\nu}\nabla_\mu n_\nu \pm q^{\mu\nu}\nabla_\mu s_\nu. \tag{21}$$

To rewrite the first term, we use the relation

$$q^{\mu\nu} = \gamma^{\mu\nu} - s^\mu s^\nu, \tag{22}$$

to get

$$q^{\mu\nu}\nabla_\mu n_\nu = \gamma^{\mu\nu}\nabla_\mu n_\nu - s^\mu s^\nu \nabla_\mu n_\nu. \tag{23}$$

Now we can add the definition of the extrinsic curvature: $K_{\mu\nu} = -\gamma^\alpha_\mu \gamma^\beta_\nu \nabla_\alpha n_\beta$ with its trace $K = \gamma^{\mu\nu} K_{\mu\nu} = -\gamma^{\mu\nu}\nabla_\mu n_\nu$, to get the relation

$$q^{\mu\nu}\nabla_\mu n_\nu = -K - s^\mu s^\nu \nabla_\mu n_\nu. \tag{24}$$

Finally, we use the property that s^μ is tangent to the 3-slice, giving $s^\mu s^\nu \nabla_\mu n_\nu = -K_{ij} s^i s^j$. Using that we can rewrite the first term to:

$$q^{\mu\nu}\nabla_\mu n_\nu = -K + K_{ij} s^i s^j. \tag{25}$$

For the second term we use that s^μ is completely on the 3-slice, meaning that we can say $s^\mu = \gamma^\mu_\alpha s^\alpha$. This means we can separate the second term into two more terms:

$$q^{\mu\nu}\nabla_\mu s_\nu = \gamma^{\mu\nu}\nabla_\mu s_\nu - s^\mu s^\nu \nabla_\mu s_\nu. \tag{26}$$

For the latter of these ($s^\mu s^\nu \nabla_\mu s_\nu$) we can use the relation $\nabla_\mu (s^\nu s_\nu) = 0$ since $s^\nu s_\nu = 1$. Rewriting this and contracting with s^μ gives $s^\mu s^\nu \nabla_\mu s_\nu = 0$, so the latter term disappears. The former does not become 0, but can be rewritten using the definition $D_\alpha s_\beta = \gamma^\mu_\alpha \gamma^\nu_\beta \nabla_\mu s_\nu$. This gives $\gamma^{\mu\nu}\nabla_\mu s_\nu = \gamma^{\alpha\beta}\gamma^\mu_\alpha \gamma^\nu_\beta \nabla_\mu s_\nu = \gamma^{\alpha\beta} D_\alpha s_\beta = D_i s^i$, meaning that the second term can be written as:

$$q^{\mu\nu}\nabla_\mu s_\nu = D_i s^i. \tag{27}$$

Since we want to know when light can't escape our black hole, we are interested in the outgoing light rays, represented by Θ_+. Now, let's take a look at what our equation for the expansion of outgoing light rays tells us, term for term

$$\underbrace{\Theta_+}_{\substack{\text{expansion}\\ \text{of light}}} = \underbrace{D_i s^i}_{\substack{\text{intrinsic}\\ \text{surface curvature}}} + \underbrace{K_{ij} s^i s^j}_{\substack{\text{outward}\\ \text{deformation}}} - \underbrace{K}_{\substack{\text{mean spacetime}\\ \text{expansion}}}. \tag{28}$$

So the first term describes how the expansion of light is affected by the spatial geometry at any point in time. The last two terms describe how the expansion of light is affected from the changes in the spacetime as time goes on. Let's look at how that plays out for a spacetime that would not have apparent horizons if it were only for the spatial geometry.

Example

What would Θ_+ be for a flat, expanding universe?

For example, we can take the FRW[13] spacetime:

$$ds^2 = -dt^2 + a(t)^2 \delta_{ij} dx^i dx^j. \tag{29}$$

Then we have

$$K_{ij} = -H\gamma_{ij}, \tag{30}$$

$$K = -3H, \tag{31}$$

with $H = \frac{\dot{a}}{a}$. For an expanding universe we have $H > 0$. This gives us

$$\Theta_+ = D_i s^i - H\gamma_{ij} s^i s^j + 3H. \tag{32}$$

For our second term, we use the fact that γ_{ij} is the metric for s^i, so it acts as a raising/lowering operator: $\gamma_{ij}s^is^j = s^is_i = 1$. That gives us

$$\Theta_+ = D_is^i + 2H. \tag{33}$$

So the expansion is positive due to the expansion of the universe. Even if the spacetime does not have any curvature, outward light rays will still diverge, as is depicted in figure 8.

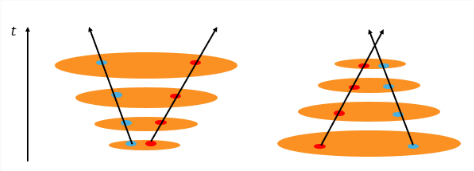

Figure 8: Flat spacetimes that are either expanding (left) or shrinking (right). This causes positive expansion for light rays on the left side and negative expansion on the right side.

What about a contracting universe?

In that case $H < 0$, so we get

$$\Theta_+ = D_is^i + \text{negative addition}. \tag{34}$$

So even if a spacetime has some kind of curvature that would cause light to diverge, it can be repressed or even overshadowed by the contracting universe. In that case, the outward light rays will converge, giving us **trapped surfaces**.

2.7 Trapped Surfaces and MOTS

As mentioned before, we want to define a horizon on our black hole, but we want to do it in a way that doesn't have the same limits as the event horizon. We will use trapped surfaces to construct this new horizon.

Trapped surfaces are defined as surfaces in the slice where light rays have negative expansion[7]. This means that they will converge, and in the case of a black hole, never escape the black hole. We can also define a border around these: the Marginally Outer Trapped Surface (MOTS)[5], where the expansion of the outgoing light rays is zero, so $\Theta_+ = 0$[3] and the expansion of the ingoing light rays is negative: $\Theta_- < 0$. We can then define the apparent horizon as the outermost MOTS in a slice, so the furthest a light ray can be, and yet still be trapped. Since we defined the MOTS purely on a slice, we can compute the apparent horizon without knowing the entire time evolution of the spacetime. This also means that the apparent horizon can change through time. Important to note is that the apparent horizon is slicing dependent, since the ADM variables are not physical fields, but gauge choices. The slicing dependence has been built into the formalism from the start.

In non-dynamic (stationary) black holes, the teleological problem with the event horizon disappears: since the spacetime never changes, knowing its entire future evolution is trivial — it looks the same as it does now, forever. The event horizon remains globally defined, but that global definition is no longer an obstacle. And since the apparent horizon was built to track the same physical boundary as the event horizon, just via a different (local, slice-based) definition, the two actually coincide in this case: for stationary black holes like Schwarzschild or Kerr, the apparent horizon overlaps exactly with the event horizon, and — like the event horizon — becomes slicing-independent. We will use this coincidence later as a check on our numerical results.

3 Method

The calculation of the apparent horizons in this project can be divided into two parts: the analytical and numerical part. In the analytical part, I calculated the shift, lapse, induced metric and extrinsic curvature of the metric using Mathematica. I then fed these values into a simulation that found the best-fitting MOTS. In this section I will describe both parts in a bit more detail. The corresponding code can be found in this repository.

3.1 Mathematica

The most challenging part of this calculation was finding a way to keep the computation time feasible. Due to technical limits regarding the licensing, Mathematica could only run for 12 hours at a time, so this put an upper limit on the calculation time. Eventually, the Riemannian Geometry & Tensor Calculus (RGTC)[14] package turned out to be the best way of calculating the covariant derivatives needed for the computation.

Due to the construction of the MOTSfinder, the metric used needed to be in quasi-Cartesian coordinates. This led us to use the Kerr-Vaidya metric in Kerr-Schild coordinates:

$$g_{\mu\nu} = \delta_{\mu\nu} + 2Hl_\mu l_\nu, \tag{35}$$

with

$$H = \frac{M(v)r}{r^2 + a^2\frac{z^2}{r^2}} \tag{36}$$

and

$$l_\mu = (1, \frac{rx + ay}{r^2 + a^2}, \frac{ry - ax}{r^2 + a^2}, \frac{z}{r}). \tag{37}$$

This expression contains $M(v)$, which needs to be converted to quasi-Cartisian coordinates. The coordinate v is the advanced time coordinate, defined by $v = t + r$. Initially, I replaced this with $M(t, r)$ to allow for the most general coordinate slicings, but after review this turned out to be more complicated than it needed to be. Switching to $M(t + r)$ still allows different slicings, but reduces the number of derivatives, which reduces the total computation time.

Another important step to reduce the calculation time was to switch to implicit differentiation. One of the things that made the calculation quite complicated was the following property of the Kerr metric:

$$\frac{x^2 + y^2}{r^2 + a^2} + \frac{z^2}{r^2} = 1. \tag{38}$$

So the radius r is not given by the trivial relation $r^2 = x^2 + y^2 + z^2$, but a more complex relation, that quickly increased calculation time when written out in the form

$$r = \frac{\sqrt{-a^2 + x^2 + y^2 + z^2 + \sqrt{4a^2z^2 + (a^2 - x^2 - y^2 - z^2)^2}}}{\sqrt{2}}, \tag{39}$$

especially when a derivative needed to be taken of this. To solve this we made use of implicit differentiation, which starts with a function derived from the original relation:

$$F(x, y, z, r) \equiv \frac{x^2 + y^2}{r^2 + a^2} + \frac{z^2}{r^2} - 1, \tag{40}$$

which we know should equal zero. Then using the chain rule we get:

$$\frac{\partial F}{\partial x}\frac{\partial x}{\partial x}+\frac{\partial F}{\partial r}\frac{\partial r}{\partial x}=0, \tag{41}$$

for the derivative with respect to x. Some algebra then gives us the relation

$$\frac{\partial r}{\partial x}=-\frac{F_x}{F_r}, \tag{42}$$

in which F_x denotes the derivative of F with respect to x and similarly for F_r. This meant that we could replace the time-intensive derivative of r with derivatives of F, which are much faster to compute.

With these additions, the total computation time reduced from over 12 hours to just under a minute, which was a lot more feasible. With the computation now feasible, the remaining task was to check that it was correct. In an ideal world we would use the Hamiltonian and Momentum constraints to check our calculation, however these took too long and couldn't be shortened. To still have somewhat of a check on the results, I compared the outcomes with the extrinsic curvature of the Schwarzschild case by putting $M = const$ and $a = 0$. The Schwarzschild case is a lot less complicated and can therefore be calculated by hand, which I have also done. The results matched, also in the funky slicing case, which provided confidence in the calculations.

The resulting expressions for the shift, lapse, induced metric and extrinsic curvature of the Kerr metric in slicing with $t =$ constant and $\tau = t + f(z) =$ constant are rather cumbersome and therefore not shown explicitly here. However, their explicit expressions can be found in the Mathematica notebook Kerr_Funky_Slicing_Final.nb.

3.2 MOTSfinder

The MOTSfinder[15] code uses an algorithm to find MOTS numerically. It requires the intrinsic metric, extrinsic curvature and the lapse and shift and their time derivatives and then finds the best-fitting MOTS. It doesn't have a built-in way to calculate MOTS of dynamic black holes in different timeslices, but that can easily be added in the surrounding Python code. My method for doing so was by adding a for-loop around the calculation of the MOTS, with every iteration of the loop representing one time slice. The way I structured the code made it possible to decide on the mass function, the slicing function $f(z)$ in the slicing $\tau = t + f(z)$ (so $f(z) = -\alpha z$ in terms of α), the rotation parameter a and the number of timeslices and time between them. This also made it possible to go back to simpler metrics, like Schwarzschild, Vaidya or Kerr, to check the outcomes with known MOTS.

4 Results

Let's first look at the MOTSfinder's output for simpler metrics, to build confidence in the calculations before moving to the full Kerr-Vaidya case. Let's first start with the non-dynamic case, as these should coincide with the event horizon, which can be analytically computed quite easily.

4.1 Checks with non-dynamic cases

The simplest case of them all: Schwarzschild. We start with a constant $M = 1$, standard slicing and no rotation, so the case where t = constant in equation 7. Since this is a non-dynamic black hole we should expect the apparent horizon to coincide with the event horizon, given by $r_{EH} = 2M$, which is indeed the case as is illustrated in 9.

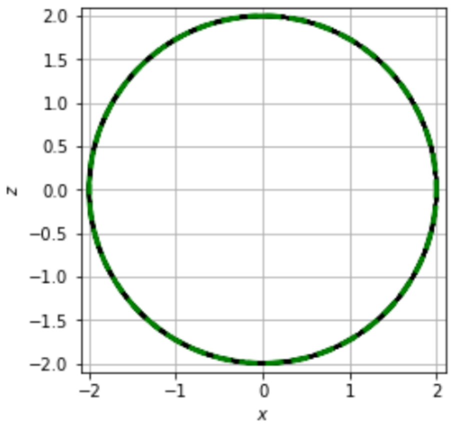

Figure 9: The apparent horizon of a Schwarzschild black hole (black line), with the event horizon (green dashed line).

Now let's add some complexity: rotation. Since this is still a non-dynamic black hole we only expect one horizon per black hole, so to make it a bit more interesting I've plotted the horizons of multiple black holes with increasing rotation parameters in one figure, see figure 10. The dashed green lines represent the event horizon for the Kerr metric with $a = 0.0$ and 0.8, which are given by[16]:

$$\begin{cases} x(\theta) = \sqrt{r_{EH}^2 + a^2 \sin(\theta)} \\ z(\theta) = r_{EH} \cos(\theta) \end{cases}, \tag{43}$$

with

$$r_{EH} = M_0 + M_0\sqrt{1 - a^2}. \tag{44}$$

In this case $M_0 = 1$. They line up very nicely with the corresponding simulated apparent horizons, as expected in a non-dynamic black hole like Kerr. The result of a higher spin parameter is also clearly visible, as it flattens the black hole along the z-axis.

Now let's add another layer of complexity: the funky slicing. Still only in a Kerr spacetime, I've plotted the apparent horizons of black holes with a constant rotation parameter ($a = 0.5$) but with increasingly extreme slicing (Fig. 11). In this case the slicing is given by $\tau = t - \alpha z$, with α the slicing factor. As this is still a non-dynamic case, the apparent horizons should and do overlap with the event horizon. The event

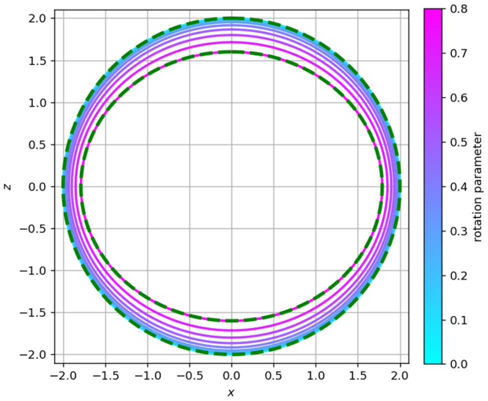

Figure 10: The apparent horizons of Kerr black holes with different rotation parameters. The event horizons for $a = 0$ and $a = 0.8$ are represented as the dashed green line.

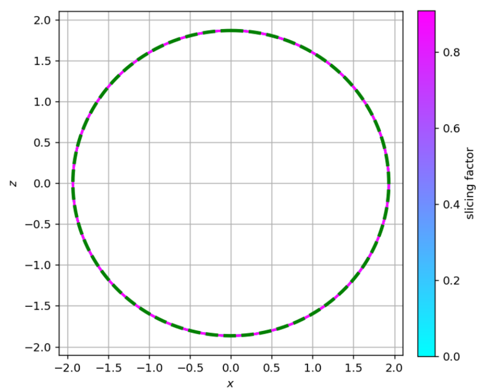

Figure 11: The apparent horizons of a Kerr black hole with a=0.5 with different slicing factors, mixing the t and z coordinates. The green dashed line represents the event horizon for the corresponding rotation parameter.

horizon is slicing-independent because it is nicely globally defined, so this means that the apparent horizon is also slicing-independent in this case. This is exactly what we find here (Fig. 11). Since the results behave exactly as predicted in these cases, this gives us confidence in our calculations and results.

4.2 Dynamic black holes

Now we can add some dynamic cases, starting with just Vaidya. As a mass function I chose a short pulse function, representing an influx of radiation that forms a black hole with final mass M_0, following the work of [1]:

$$M(t+r) = \begin{cases} 0 & \text{for } t+r \leq 0 \\ M_0(t+r)^2/((t+r)^2+W^2) & \text{for } t+r > 0 \end{cases}. \tag{45}$$

In the case of just Vaidya, the values chosen by [1] result in the apparent horizons being very bunched up close together, which makes the pulse effect difficult to see. To make this more visible I chose some larger values, in this case $M_0 = 2$ and $W = 5$. The resulting mass function can be seen in figure 12. This gave the apparent horizons shown

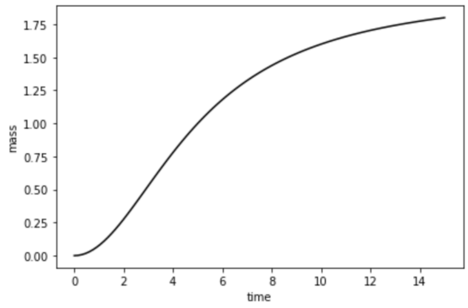

Figure 12: The mass function in the Vaidya spacetime of figure 13, based on equation 45 with values $M_0 = 2$ and $W = 5$.

in figure 13. The apparent horizons again behave exactly as we expect them to. They

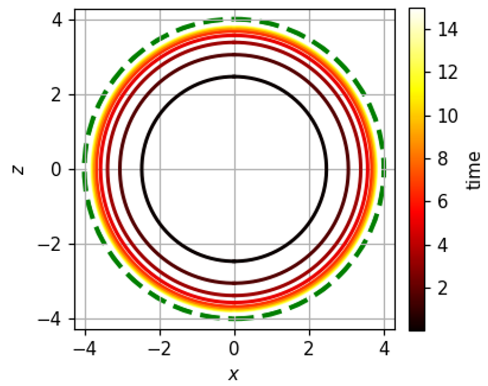

Figure 13: The apparent horizons of a Vaidya black hole through time, represented by the solid lines. The green dashed line represents the event horizon for a Schwarzschild black hole of $M = M_0 = 2$.

get larger as the mass increases, yet never larger than the event horizon at the maximum mass. The quick increase of the mass function can also be recognized in the larger space between the first few horizons compared to the space between those at a later time.

Now let's take a look at the funky slicing. In this case the values chosen by [1] do give a clear picture, so I have used them as well. They are $M_0 = 1$, $W = \frac{1}{10}$ and the slicing factor is $\alpha = \frac{10}{11}$. This gives a rather extreme slicing. The mass function is given in figure 14. The resulting apparent horizons are shown in figure 15. The effect of the funky slicing can be seen at the top of the figure, where the slicing clearly mixes the time and z-coordinates. As we go further in time, this effect becomes weaker and eventually the apparent horizon seems to approach the shape of the event horizon.

To make sense of this behaviour we need to look at the mass function of the black hole. As time goes on, the mass function starts to converge to M_0. Once it fully converges to M_0, we would expect the black hole to essentially behave as a Schwarzschild black hole with $M = M_0$, including having its apparent horizon overlap with the event horizon. At that point, the apparent horizon should be slicing-independent again. So,

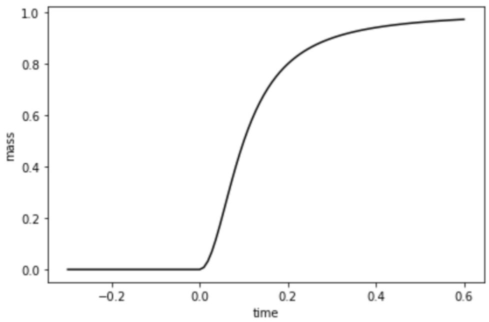

Figure 14: The mass function in the Vaidya spacetime of figure 15, based on equation 45 with values $M_0 = 1$ and $W = \frac{1}{10}$. The label "time" refers to τ, the new time coordinate in the funky slicing.

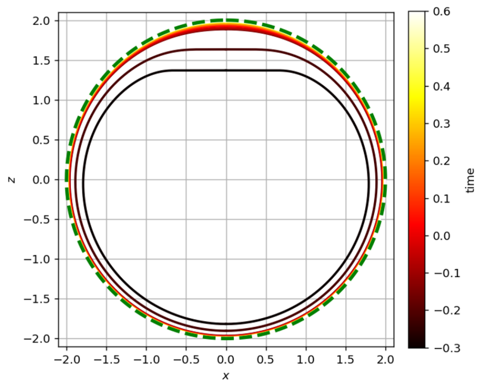

Figure 15: The apparent horizons of a Vaidya black hole with funky slicing, represented by the solid lines. The time axis represents τ, the time coordinate after taking the funky slicing. The green dashed line represents the event horizon for a Schwarzschild black hole of $M = M_0 = 1$.

as the mass function starts to approach M_0, essentially becoming "less dynamic", the effect of the funky slicing starts to become weaker.

This all behaves exactly as expected, so now we can look at the whole picture and add all the complexities together. This forms the Kerr-Vaidya black hole with funky slicing. The parameters for the mass function and the slicing are kept the same as in the previous result, with now an additional rotation parameter of $a = 0.5$. In this case, the event horizon for comparison is based on a Kerr black hole with mass M_0 and the same rotation parameter. The results can be found in figure 16. We can see the same effects of the funky slicing and mass function as in the previous results, with the added flattening caused by the rotation. Again, this aligns very nicely with the event horizon for Kerr in the limit of $M \to M_0$.

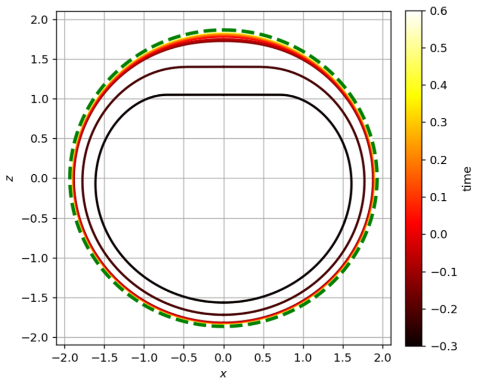

Figure 16: The apparent horizons of a Kerr-Vaidya black hole with funky slicing, represented by the solid lines. The time axis represents τ, the time coordinate after taking the funky slicing. The green dashed line represents the event horizon for a Kerr black hole of $M = M_0 = 1$ and $a = 0.5$.

4.3 Discussion

Although my results behave exactly as expected, it is important to be aware of possible mistakes that can easily slip in, especially in such large computations. Ideally, I would have liked to check the Hamiltonian and momentum constraints to make sure that my Mathematica calculation was correct, but this added too much calculation time. Although reproducing the Schwarzschild and Kerr horizons gives confidence in the implementation, it does not constitute a complete verification of the Mathematica calculations. It remains possible that subtle errors only become apparent in the fully dynamical Kerr-Vaidya case.

In this project I've focussed on the Kerr-Vaidya black holes. This is a good test case for dynamic black holes, since it does have *some* complexity, but it is still analytically manageable. This will provide a good stepping stone for more complicated, more realistic black holes, which are studied using numerical simulations.

In this project, I have limited myself to only computing one family of funky slicings, that still leaves an axisymmetrical computation. Adding different slicings that break this symmetry would add in complexity but would also add a lot of new insights into the behaviour of apparent horizons. Since I've only investigated one type of slicing - other than the " normal one", it remains unclear whether the observed behaviour is generic or specific to this particular funky slicing. I also discussed only one mass function. I have tried a few more that also behave as expected, but haven't looked at this with much detail, which could also be valuable. Furthermore, the conclusions drawn from the results are based on optical review of the plots. To definitively verify whether the apparent horizons match with the event horizons, it would have been better to also check this quantitatively. An additional review of these values would strengthen my conclusions.

4.4 Outlook

Now that we know that the calculations and simulations produce the expected results, we can use them to learn more about how these apparent horizons behave. Some interesting next steps include:

Horizontal funky slicing
In this project I chose to place my funky slicing on the z-axis: $\tau = t - \alpha z$, but another interesting choice would be $\tau = t - \alpha x$. Since this would break the equatorial symmetry in the Kerr black hole, this might yield some interesting results.

Spherical harmonics
Another interesting next step would be to decompose the results into spherical harmonics. Due to technical problems, this was sadly not feasible within this project, but this could lead to valuable insights, since this would make it possible to see repeating patterns in the horizons across different slicings.

Geometric properties
Thus far I've only looked at the location of the apparent horizon, not its geometric properties, like the shear. It could be worth investigating these, as they might reveal more properties of apparent horizons.

4.5 Conclusion

To summarise, in my master's project I have successfully computed the apparent horizon of a Kerr-Vaidya black hole for multiple slicings. We have seen that the apparent horizons change depending on that slicing. This is exactly what we expect, because the apparent horizon is defined locally on each slice rather than globally like the event horizon. Although the apparent horizon is not a globally defined geometric object, its dependence on the chosen slicing is precisely what makes it suitable for numerical relativity. Unlike the event horizon, it can be located using only local information on a single timeslice, making it a practical tool for studying dynamical black holes. My results can be used to further examine these horizons in even funkier slicings and hopefully understand more about the behaviour of apparent horizons in different timeslices.

References

[1] Erik Schnetter and Badri Krishnan. "Nonsymmetric trapped surfaces in the Schwarzschild and Vaidya spacetimes". In: *Physical Review D* 73.2 (Jan. 2006). ISSN: 1550-2368. DOI: 10.1103/physrevd.73.021502. URL: http://dx.doi.org/10.1103/PhysRevD.73.021502.

[2] Robert M. Wald. *General Relativity*. Chicago, USA: Chicago Univ. Pr., 1984. DOI: 10.7208/chicago/9780226870373.001.0001.

[3] Jonathan Thornburg. "Event and Apparent Horizon Finders for 3 + 1 Numerical Relativity". In: (2007). DOI: 10.12942/lrr-2007-3. URL: https://doi.org/10.12942/lrr-2007-3.

[4] Abhay Ashtekar and Badri Krishnan. "Quasi-local black hole horizons: recent advances". In: *Living Reviews in Relativity* 28.1 (Oct. 2025). ISSN: 1433-8351. DOI: 10.1007/s41114-025-00061-4. URL: http://dx.doi.org/10.1007/s41114-025-00061-4.

[5] Lars Andersson, Marc Mars, and Walter Simon. "Local Existence of Dynamical and Trapping Horizons". In: *Physical Review Letters* 95.11 (2005). ISSN: 1079-7114. DOI: 10.1103/physrevlett.95.111102. URL: http://dx.doi.org/10.1103/PhysRevLett.95.111102.

[6] Robert M. Wald and Vivek Iyer. "Trapped surfaces in the Schwarzschild geometry and cosmic censorship". In: *Phys. Rev. D* 44 (12 Dec. 1991), R3719(R)–R3722(R). DOI: 10.1103/PhysRevD.44.R3719. URL: https://link.aps.org/doi/10.1103/PhysRevD.44.R3719.

[7] S. W. Hawking and G. F. R. Ellis. *The Large Scale Structure of Space-Time*. Cambridge Monographs on Mathematical Physics. Cambridge University Press, 1973.

[8] Eric Poisson. *A Relativist's Toolkit: The Mathematics of Black-Hole Mechanics*. Cambridge University Press, 2004.

[9] Pravin Kumar Dahal and Daniel R. Terno. "Kerr–Vaidya black holes". In: *Physical Review D* 102.12 (Dec. 2020). ISSN: 2470-0029. DOI: 10.1103/physrevd.102.124032. URL: http://dx.doi.org/10.1103/PhysRevD.102.124032.

[10] Eric Gourgoulhon. *3+1 Formalism and Bases of Numerical Relativity*. 2007. arXiv: gr-qc/0703035 [gr-qc]. URL: https://arxiv.org/abs/gr-qc/0703035.

[11] Alejandro Corichi and Dario Núñez. "Introduction to the ADM formalism". In: (2022). eprint: arXiv:2210.10103.

[12] Josu C. Aurrekoetxea, Katy Clough, and Eugene A. Lim. "Cosmology using numerical relativity". In: *Living Reviews in Relativity* 28.1 (June 23, 2025), p. 5. ISSN: 1433-8351. DOI: 10.1007/s41114-025-00058-z. URL: https://doi.org/10.1007/s41114-025-00058-z.

[13] Sean M. Carroll. *Spacetime and Geometry: An Introduction to General Relativity*. Cambridge University Press, 2019.

[14] S. Bonanos. "Capabilities of the Mathematica Package 'Riemannian Geometry and Tensor Calculus' (RGTC)". In: *Proceedings of the 10th Italian Conference on General Relativity and Gravitational Physics*. World Scientific, 2001, pp. 227–236. URL: http://www.inp.demokritos.gr/~sbonano/RGTC/.

[15] B. Krishnan D. Pook-Kolb O. Birnholtz and E. Schnetter. *Existence and stability of marginally trapped sufraces in black-hole spacetimes*. 2019. DOI: 10.1103/PhysRevD.99.064005. URL: https://link.aps.org/doi/10.1103/PhysRevD.99.064005.

[16] Matt Visser. *The Kerr spacetime: A brief introduction*. 2008. arXiv: 0706.0622 [gr-qc]. URL: https://arxiv.org/abs/0706.0622.